Biosensors and Bioelectronics 120 (2018) 1–7

Contents lists available at ScienceDirect

Biosensors and Bioelectronics

journal homepage: www.elsevier.com/locate/bios

Ultrasensitive photoelectrochemical immunosensor for the detection of amyloid β-protein based on $SnO_2/SnS_2/Ag_2S$ nanocomposites

Yaoguang Wang[a], Dawei Fan[a], Guanhui Zhao[a], Jinhui Feng[a], Dong Wei[b], Nuo Zhang[a,*], Wei Cao[a], Bin Du[a,b], Qin Wei[a,*]

[a] Key Laboratory of Interfacial Reaction & Sensing Analysis in Universities of Shandong, School of Chemistry and Chemical Engineering, University of Jinan, Jinan 250022, PR China

[b] School of Water Conservancy and Environment, University of Jinan, Jinan 250022, PR China

ARTICLE INFO

Keywords:
Label-free
Photoelectrochemical immunosensor
Alzheimer's disease
Amyloid β-protein
$SnO_2/SnS_2/Ag_2S$ nanocomposites

ABSTRACT

An ultrasensitive label-free photoelectrochemical (PEC) immunosensor with high visible-light activity was developed for quantitative detection of amyloid β-protein (Aβ) by cross-linking anti-Aβ antibody onto the Ag_2S sensitized SnO_2/SnS_2 nanocomposites. Specifically, SnO_2 with flower-like porous nanostructure was innovatively applied in PEC immunosensor as a basal material. It could form a heterostructure with SnS_2, which brought about the sensitization of SnO_2 and enhanced the separation of photogenerated electrons and holes. Moreover, Ag_2S was in-situ growth on the surface of SnO_2/SnS_2, which further enhanced the photocurrent response significantly. Therefore, $SnO_2/SnS_2/Ag_2S$ could form stepwise band-edge structure, which benefited the light harvesting and provided a good foundation for sensor construction and detection. Under optimal conditions, the PEC immunosensor was used to detect the content of Aβ and exhibited a wide linear concentration range from 0.5 pg mL^{-1} to 100 ng mL^{-1}, with low limit of detection (0.17 pg mL^{-1}) and limit of quantification (0.56 pg mL^{-1}). Additionally, the designed PEC immunosensor exhibited good reproducibility, specificity, and stability which may find potential applications in the biosensor, biomedicine, clinical diagnosis, photocatalysis and other related fields.

1. Introduction

Alzheimer's disease (AD) is an insidious and chronic neurodegenerative disorder causing memory decline and dysfunction of cognitive functions, with no effective disease-modifying therapy available currently (Cummings, 2004; Thapa et al., 2016). The amyloid-β protein (Aβ) has been proposed as the trigger for a cascade of events in the brain that lead to AD for 27 years (Selkoe and Hardy, 2016). Although the precise neurotoxic mechanism remains to be controversial, genetic, biochemical, molecular biological and pathological evidence strongly supported the amyloid hypothesis, positing that the excessive accumulation of Aβ is the primary pathological event leading to neurofibrillary tangles, neurodegeneration and neuroinflammation in AD. In recent years, a growing number of amyloid β-protein antibody (anti-Aβ) treatments have been developed to short-circuit this cascade, and several are currently being evaluated in people who have already developed or are at risk of developing symptoms of Alzheimer's (Reiman, 2016). But there are no treatments available that prevent this condition. Actually, Aβ is deposited early in the disease process decades prior to symptoms. Specifically, Aβ levels are detected in preclinical disease stages and can predict future cognitive decline and neurodegeneration. An Aβ concentration of < 500 pg mL^{-1} is indicative that Aβ is accumulating in the brain (Carneiro et al., 2017). Thus, Aβ is a very useful biomarker for confirming whether the patient has a good or bad prognosis for AD and ultralow concentration detection of Aβ is of great importance. Moreover, ultralow concentration detection of Aβ is required, which is because that the low limit of detection (LOD) could undoubtedly improve the detection accuracy and reduce the amount of sample required. Therefore, there is a continuing demand for fast and simple analytical methods for the determination of Aβ.

Many studies have been reported on the detection of carcinoembryonic antigen (CEA), prostate specific antigen (PSA), α-fetoprotein (AFP), squamous cell carcinoma antigen (SCCA), insulin and other disease markers by photoelectrochemical (PEC) sensor (Fan et al., 2015; Han et al., 2018; Lv et al., 2018; Qiu et al., 2018; Wang et al., 2017b, 2017c; Zhao et al., 2012). As far as we know, few researches have been reported for detecting Aβ by label-free PEC method. Compared with conventional optical methods, the PEC immunoassay is particularly

* Corresponding authors.
E-mail addresses: zhangnuoujn@163.com (N. Zhang), sdjndxwq@163.com (Q. Wei).

https://doi.org/10.1016/j.bios.2018.08.026
Received 30 June 2018; Received in revised form 9 August 2018; Accepted 11 August 2018
Available online 13 August 2018
0956-5663/

attractive in the field of diagnosis because it can unite the specificity and affinity of the antibody-antigen reaction with the inherent characteristics of electrochemical techniques such as high sensitivity, low cost, easy miniaturization, and so on. Furthermore, no researches have been done by using PEC method for the detection of Aβ based on SnO_2/SnS_2/Ag_2S modified ITO electrode.

As is known to all, metal oxide nanomaterials have attracted tremendous attention in the field of PEC immunosensor, which have shown excellent capability to detect trace concentrations of various environmental pollutants and tumor markers. In recent years, various semiconductor materials have been exploited as the substrate for the PEC sensor. Tin dioxide (SnO_2), a typical representative of metal oxide semiconductor nanomaterials, has received considerable attentions owning to its controllable morphology, environmental friendliness, large surface area, excellent photoelectronic properties and low cost (Jiang et al., 2018). Different external environmental parameters and reaction conditions can change the morphology of SnO_2 to a certain extent, such as SnO_2 nano-microspheres, SnO_2 nanoparticles, SnO_2 nanoflowers and other microstructures. Therefore, SnO_2 as a stable n-type wide band-gap semiconductor (Eg = 3.6 eV) has been intensively explored for various applications in transparent electrode, gas sensor, electrochemical luminescence sensor, rechargeable lithium-ion battery and solar cell (Elangovan and Ramamurthi, 2003; Huang et al., 2018; Shi and Lin, 2011; Wang et al., 2018a, 2006; Yan et al., 2018; Yin et al., 2018). However, very few reports of SnO_2 in PEC sensors were shown, especially when the ultrathin SnO_2 nanosheets aggregated to form flower-like nanostructure with better sensing properties.

It is now accepted that using semiconductors composites can improve photocatalytic activity compared with using a single semiconductor, which is due to the effective separation of photogenerated electrons (e^-) and holes (h^+) (Cao et al., 2011; Ma et al., 2014; Xie et al., 2017; Zhang et al., 2009; Zhou et al., 2010). Stannic sulfide (SnS_2) has been known as good semiconductor photocatalytic materials with its narrow band-gap (~ 2.3 eV) and has been used for photoelectric sensor under visible light irradiation because of its low toxicity, low relative cost and wide spectral response (Banerjee et al., 2008). SnO_2 can form a heterostructure with SnS_2, which brings about the sensitization of SnO_2 and enhances the separation of photogenerated electrons and holes (Yao et al., 2014; Zhang et al., 2018; Zhou et al., 2012). Moreover, SnO_2 possessed superior electron mobility and the very positive valence band position which can prevent hole back-transfer through the SnO_2 layer and forms a 'hole mirror' (Liang et al., 2011; Zhang et al., 2011).

Meanwhile, semiconducting metal sulfides such as CdS, Ag_2S and MoS_2 have relatively narrow band-gaps and thus are capable of harvesting photons in the visible range, which are widely used in photocatalysts (Liu et al., 2011; Yang et al., 2012; Yun et al., 2016). Recently, Ag_2S nanoparticles have attracted many interests owing to their narrow band-gap (~ 1.0 eV), negligible toxicity, good electron transfer efficiency and relatively high visible-light absorption (Liu et al., 2015; Park et al., 2015). Ag_2S nanoparticles can be applied to construct a stepwise structure of band-edge levels in the SnO_2/SnS_2 electrode because of their harmonious band-gaps, which can promote ultrafast transfer charge and effectively inhibited the e^-/h^+ pair recombination.

In this study, we synthesized pure flower-like hierarchical SnO_2 nanosheets by combining a facile hydrothermal and calcination method. At the same time, the hierarchical nanosheet structure exhibited large surface area, strong adsorption capacity, good biocompatibility and excellent sensing properties. In fact, as a basal material, SnO_2 showed good load performance and can firmly attach to the electrode surface. Moreover, Ag_2S nanoparticles can be applied to construct a stepwise structure of band-edge levels in the SnO_2/SnS_2 electrode because of their harmonious band-gaps. Ag_2S nanoparticles were loaded on the surface of SnO_2/SnS_2 by in-situ growth via strong adsorption interactions between SnS_2 and Ag_2S, which enhanced the photocurrent response in the visible-light region. It was found that the SnO_2/SnS_2/Ag_2S nanocomposites could greatly enhance the photocurrent with visible light irradiation in comparison with single SnO_2, SnS_2 or SnO_2/SnS_2. Meanwhile, an ultrasensitive label-free PEC immunosensor based on Ag_2S sensitized on SnO_2/SnS_2 with high photocurrent response was fabricated by layer-by-layer (LBL) method for the first time for the quantification of Aβ, with the goal of performing a clinical diagnosis and monitor biochemical effects of AD treatments. Ascorbic acid (AA) was selected as an electron donor for scavenging photogenerated holes to suppress photogenerated e^-/h^+ recombination. The fabricated label-free PEC immunosensor exhibited a wide line arrange (0.0005–100 ng mL^{-1}) with low LOD (0.17 pg mL^{-1}) and limit of quantification (LOQ, 0.56 pg mL^{-1}), and good selectivity, reproducibility and stability, which exhibited its potential applications in many disease markers, environmental pollutants and other biological targets detection, clinical diagnosis, photocatalysis and other fields.

2. Experimental

2.1. Materials

Aβ and anti-Aβ were purchased from GenScript (Nanjing) Co., Ltd. China. Thioglycolic acid (TGA) and citric acid were obtained from Macklin Reagent Co., Ltd. (Shanghai, China). 1-ethyl-3-(3-dimethylaminopropyl) carbodiimide hydrochloride (EDC) and N-hydroxysuccinimide (NHS) were obtained from Aladdin Reagent Database Inc. (Shanghai, China). Tin (IV) chloride pentahydrate ($SnCl_4$), thioacetamide, silver nitrate ($AgNO_3$), sodium sulfide (Na_2S), ascorbic acid (AA), absolute ethanol, isopropyl alcohol and acetone were purchased from Sinopharm Chemical Reagent Co., Ltd. (Beijing, China). Phosphate buffered solutions (PBS, 1/15 mol L^{-1} KH_2PO_4 and 1/15 mol L^{-1} Na_2HPO_4) containing AA was used as an electrolyte for the PEC measurements. All other chemicals in the experiment were analytical grade and were used as received without further purification.

2.2. Apparatus

High resolution transmission electron microscopy (HRTEM) images and Energy-dispersive X-ray (EDX) elemental mapping images were obtained from a field-emission transmission electron microscope (Hitachi JEM-2100F, Japan). Scanning electron microscope (SEM) images and energy dispersive spectroscopy (EDS) were obtained by using a field-emission scanning electron microscope (SEM, Zeiss, Germany). Electrochemical impedance spectroscopy (EIS) analysis was performed with an RST5200F electrochemical workstation (Zhengzhou Shiruisi Technology Co., Ltd, China) with a three-electrode system in a 5.0 mmol L^{-1} $[Fe(CN)_6]^{3-/4-}$ solution containing 0.10 mol L^{-1} KCl. UV–vis diffuse reflectance spectrum measurements were performed with a Shimadzu UV-3101PC spectrometer (Japan). All PEC experiments were measured on a CHI760E electrochemical workstation (Chenhua Instrument Shanghai Co., Ltd, China) by using a conventional three-electrode system comprising of a saturated calomel electrode as reference electrode, a platinum wire as a counter-electrode, and the as-prepared SnO_2/SnS_2/Ag_2S modified ITO electrode (2.5 × 1.0 cm^2) as working electrode.

2.3. Synthesis of SnO_2 and SnS_2

SnO_2 and SnS_2 were prepared by the reported solvothermal method (Li et al., 2017). In detail, thioacetamide (0.048 g) and $SnCl_4$ (21 μL) were added to a 50 mL of Teflon-lined stainless steel autoclave containing 30 mL of isopropanol and sonicated until all the materials were dissolved. Afterwards, the autoclave was placed in the oven and heated at 180 °C for 24 h. After cooling to room temperature naturally, the products were rinsed with water and ethanol for at least 5 times and then dried in the oven at 80 °C overnight. Subsequently, the as-prepared SnS_2 was calcined at 500 °C for 2 h in a muffle under the air

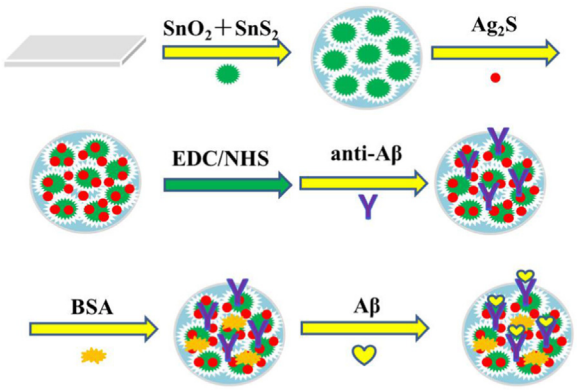

Fig. 1. Construction process of the PEC immunosensor for the detection of Aβ.

atmosphere. After cooling to room temperature, the SnS_2 precursor was converted to SnO_2 with retained nanosheet morphology.

2.4. Fabrication of the label-free PEC immunosensor

First, the ITO electrodes (2.5 × 1.0 cm^2) were successively washed for 30 min at 50 °C in series of ultrasonically solvents (acetone, ultrapure water, ethanol, and ultrapure water). The preparation process of the ultrasensitive PEC immunosensor was illustrated in Fig. 1. Typically, 6 μL of 3 mg mL^{-1} SnO_2 aqueous suspension was dropped onto a piece of ITO electrode. After the modified electrode was dried naturally, 6 μL of 5 mg mL^{-1} SnS_2 aqueous solution was dropped onto the SnO_2 modified ITO electrode and dried naturally. There was another method to prepare ITO/SnO_2/SnS_2 electrode. Firstly, SnO_2 and SnS_2 were mixed uniformly by ultrasound, and then dropped onto the ITO electrode. The as-prepared ITO/SnO_2/SnS_2 electrode was then successively soaked 3 min for each step in 0.1 mol L^{-1} $AgNO_3$ solution in alcohol in dark place and 0.1 mol L^{-1} Na_2S in methanol aqueous solution (V/V = 1:1). In this process, the ITO/SnO_2/SnS_2/Ag_2S electrode was fabricated. After that, 6 μL of 3 mmol L^{-1} thioglycolic acid (TGA) aqueous solution was dropped on the ITO/SnO_2/SnS_2/Ag_2S electrode for 1 h at room temperature, followed by rinsing to remove the excess TGA. Then 6 μL of EDC (0.01 mol L^{-1})/NHS (0.002 mol L^{-1}) aqueous solution was dropped onto ITO/SnO_2/SnS_2/Ag_2S/TGA electrode for 1 h at room temperature, followed by thoroughly rinsing with ultrapure water to remove the excess EDC/NHS. The EDC/NHS was used as the linker between the -COOH of TGA modified Ag_2S and the -NH_2 of anti-Aβ via amidation reaction. Subsequently, 6 μL of 10 μg mL^{-1} anti-Aβ solution was dropped onto the electrode surface for 30 min under the room temperature. After that, the electrode was rinsed with the washing buffer solution to remove unbound and physically adsorbed anti-Aβ. The electrode was then covered with 6 μL of 0.1% bovine serum albumin (BSA) solution for 1 h at room temperature to block nonspecific binding sites and then washed thoroughly. Next, 6 μL of different concentrations of Aβ was dropped onto the electrode for 1 h and dried. After rinsing, the ITO/SnO_2/SnS_2/Ag_2S/TGA/(EDC/NHS)/anti-Aβ/BSA/Aβ PEC immunosensor was constructed and stored at 4 °C until use.

The photogenerated e^-/h^+ transfer mechanism of the PEC immunosensor in the environment of ascorbic acid (AA) electrolyte was shown in Fig. 2. SnO_2, SnS_2 and Ag_2S possessed different optimal absorption bands due to different energy gaps, they can present cascade band-edge levels to promote ultrafast transfer of charge and effectively inhibit the recombination of e^-/h^+ pairs, which led to the enhanced photocurrent responses. AA is an excellent electron donor which can block the recombination of photogenerated holes. The specific binding of anti-Aβ with target Aβ blocked the electron transfer from AA to SnO_2/SnS_2/Ag_2S composites and resulted in the decrease of photocurrent. It is interesting to note that the photocurrent intensity

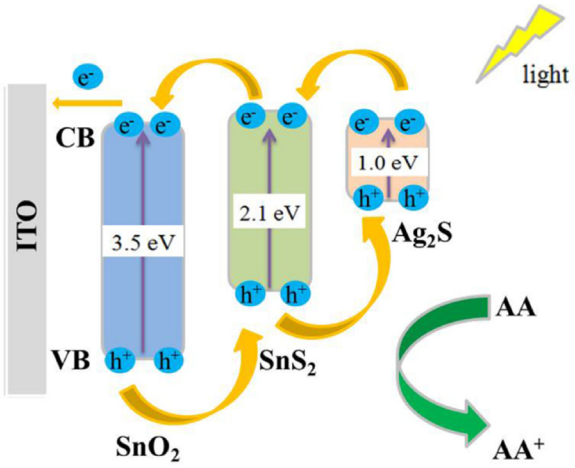

Fig. 2. Illustration of charge-transfer mechanism based on SnO_2/SnS_2/Ag_2S.

decreased gradually with the increase of Aβ concentration. Consequently, the quantitative detection of Aβ was achieved by the fabricated PEC immunosensor.

2.5. PEC detection of Aβ

PEC detection was carried out in PBS (pH = 7.4, 1/15 mol L^{-1}) containing 0.1 mol L^{-1} AA at room temperature. The AA was served as sacrificial electron donor during the photocurrent measurement. Photocurrent was measured by the current-time curve on a PEC workstation. A 100 W LED lamp (white light) was used as an irradiation source in the PEC test and was switched on and off every 10 s. The applied potential was 0 V.

3. Results and discussion

3.1. Characterization of SnO_2 and SnO_2/SnS_2/Ag_2S nanocomposites

SEM was employed to study the general morphologies and dimensions of SnO_2 and SnO_2/SnS_2/Ag_2S. As shown in Fig. 3A, the prepared SnO_2 nanomaterials displayed a hierarchical flower-like architecture with the average diameter of about 1–2 μm. In fact, the flower-like architecture was derived from the assembly of nanosheets with an ultrathin thickness. Close observation of HRTEM images of SnO_2 (Fig. 3C and D) also clearly displayed their flower-like shape, which was well consistent with the SEM results. Moreover, it revealed that the nanosheets contained numerous pores, which were formed during the calcination process. Additionally, observed from the SEM image of the SnO_2/SnS_2/Ag_2S nanocomposites (Fig. 3B), the great amounts of Ag_2S nanoparticles with a small size were covered on the surface of hierarchical flower-like architecture. It could also indicate the successful loading of Ag_2S nanoparticles on the surface of SnO_2/SnS_2 nanosheets. The EDS spectrum (Fig. 3E) exhibited the characteristic peaks of S, Sn, O and Ag, which also proved the successful synthesis of the SnO_2/SnS_2/Ag_2S nanocomposites. Furthermore, observed from Fig. S1A, SnO_2/SnS_2/Ag_2S nanocomposites also showed flower-like architecture. The EDX mapping images (Fig. S1B–E) exhibited the elements of O, S, Sn and Ag, respectively, confirming their homogenous distribution. The high overlap of elements S, Sn, and Ag in these EDX mapping images also indicated the successful formation of Ag_2S nanoparticles which covered on the flower-like architecture of SnS_2. Fig. 3F showed the UV–vis diffuse reflectance spectra of the prepared SnO_2, SnO_2/SnS_2 and SnO_2/SnS_2/Ag_2S under different conditions. The absorption wavelength of SnO_2 was clearly under 400 nm in the UV range, which was ascribed to the wide band-gap of 3.5 eV. However, SnO_2 can be coupled with SnS_2 to make the SnO_2/SnS_2 absorb and utilize visible-light

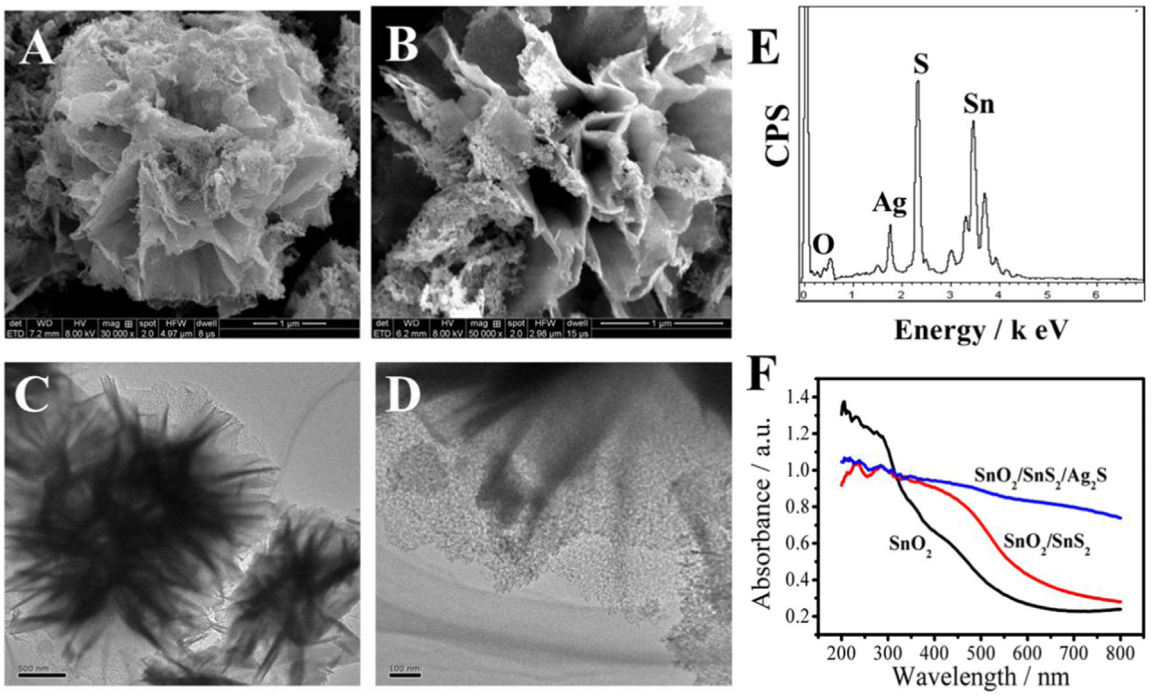

Fig. 3. SEM images of SnO_2 (A), $SnO_2/SnS_2/Ag_2S$ (B); HRTEM images of SnO_2 (C and D); EDS spectrum of $SnO_2/SnS_2/Ag_2S$ (E); UV–vis diffuse reflectance spectra of SnO_2, SnO_2/SnS_2 and $SnO_2/SnS_2/Ag_2S$ (F).

efficiently while its absorption wavelength can reach up to 650 nm. Ag_2S is small band-gap sensitizer which has the lowest band-gap energy of 1.0 eV. The deposition of Ag_2S on the SnO_2/SnS_2 led to a broad absorption in visible-light and increasing absorption intensity, which can generate the most photogenerated e^-/h^+ pairs under visible-light irradiation. Therefore, the combination of SnO_2, SnS_2 and Ag_2S can absorb light energy better and generate stronger photocurrent signal. Observed from Fig. S2, we can see that the photocurrent of $SnO_2/SnS_2/Ag_2S$ can be up to 135 μA, which was 2.6, 6.1, and 7.1 times that of the SnO_2/Ag_2S, SnS_2/Ag_2S, SnO_2/SnS_2, respectively. The ITO/$SnO_2/SnS_2/Ag_2S$ electrode showed the best excellent photoelectric property, which was selected as substrate material in this study.

3.2. Characterization of the fabricated PEC immunosensor

The modified electrodes were tested by the photocurrent response and electrochemical impedance spectroscopy (EIS) to study the state of connection between composite material and ITO electrode, further exploring the condition of building the immunosensor (Wang et al., 2018b; Xie et al., 2018; Xiong et al., 2017). In addition, in order to obtain high and stable photocurrent signal, a certain amount of ascorbic acid (AA) was added to the testing environment. AA is a widely used excellent antioxidant with the oxidation potential of − 0.185 V (vs. SCE). As the electron donation, AA can be oxidized by the holes generated by illuminated Ag_2S nanoparticles, which facilitates the separation of photogenerated e^-/h^+ to get perfect photocurrent response.

Under the visible-light excitation, the photoelectric behavior of the modified electrodes was investigated. Fig. 4A showed the photocurrent-time curve of the modified electrode which was designed as the immunosensor to detect Aβ. The photocurrent signal of bare ITO electrode was almost zero (curve a). Compared with the bare ITO, the photocurrent response of ITO/SnO_2 was also very little (curve b). After modified with SnS_2, the photocurrent signal of ITO/SnO_2/SnS_2 electrode increased to about 19 μA (curve c). The phenomenon also proved that SnS_2 has been modified on the surface of SnO_2. Exhilaratingly, the photocurrent signal of ITO/$SnO_2/SnS_2/Ag_2S$ electrode was excellent and reached to 135 μA (curve d), which indicated that Ag_2S nanoparticles grew firmly on the surface of SnO_2/SnS_2 to form the $SnO_2/SnS_2/Ag_2S$ nanocomposites with perfect PEC activity by in-situ growth method. Moreover, Ag_2S as a narrow bandwidth of semiconductor material improved the photoelectric response distinctly. When anti-Aβ (curve e), BSA (curve f) and Aβ (curve g) were modified onto the surface of the ITO electrode successively, the photocurrents reduced gradually. Protein molecules such as Aβ, BSA and anti-Aβ were insulating, which prevent AA from combining with photogenerated holes of Ag_2S. Therefore, recombination of photogenerated e^-/h^+ got more easily and resulted in a reduction of the photocurrent. As a result, when the Aβ was connected with anti-Aβ by the specific recognition between antigen and antibody, the photocurrent intensity reduced obviously from 73 μA to 35 μA. These phenomena demonstrated the successful fabrication of the PEC immunosensor based on $SnO_2/SnS_2/Ag_2S$ nanocomposites for the detection of Aβ.

To deeply analyze the construction processes of the label-free PEC immunosensor, the EIS analysis was carried out in the solution of 5.0 mmol L^{-1} $[Fe(CN)_6]^{3-/4-}$ including 0.1 mol L^{-1} KCl. The EIS Nyquist plots of layer-by-layer modified ITO electrodes were shown in Fig. 4B. Typically, EIS diagram consists of two parts: one part is the restrictions in the process of high frequency semicircle part; the other part is the linear part of low frequency in the process of diffusion. The diameter of the semicircle in the high frequency part can directly reflect the electrode transfer resistance (R_{et}) value (Hu et al., 2018; Wang et al., 2017a). The R_{et} value of bare ITO electrode was small because of its certain conductivity (curve a). When modifying SnO_2 (curve b), SnS_2 (curve c) on the ITO, the R_{et} value increased significantly, implying their successful fabrication on ITO electrode. After the combination of Ag_2S on ITO/SnO_2/SnS_2 surface (curve d), perhaps because of the electrostatic adsorption between Ag_2S and $[Fe(CN)_6]^{3-/4-}$, the electron transfer of the electronic mediator was accelerated and the conductivity was improved, which led to the significant decrease of R_{et} value. The R_{et} value increased gradually after successive modification with anti-Aβ (curve e), BSA (curve f) and Aβ (curve g) because of the hindrance and insulation property of protein. In general, these results demonstrated that the proposed PEC immunosensor has been fabricated successfully and could be applied for the determination of Aβ.

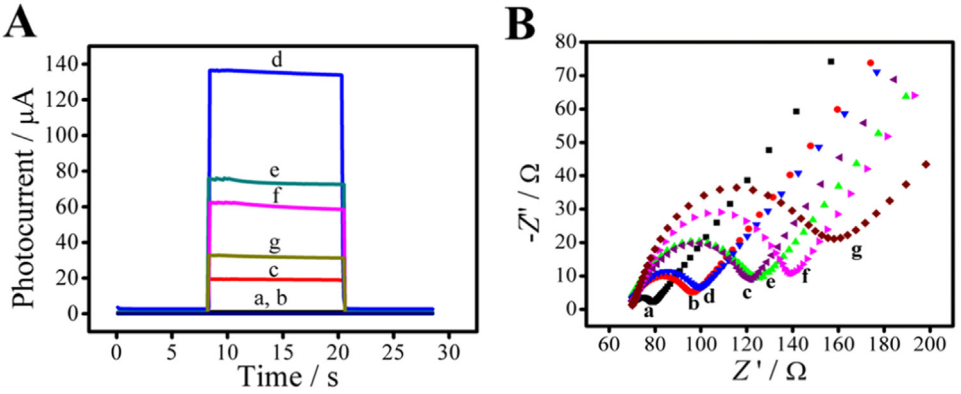

Fig. 4. Time-based photocurrent response curves (A) and EIS Nyquist plots (B) of ITO electrode (a), ITO/SnO_2 (b), ITO/SnO_2/SnS_2 (c), ITO/SnO_2/SnS_2/Ag_2S (d), ITO/SnO_2/SnS_2/Ag_2S/anti-Aβ (e), ITO/SnO_2/SnS_2/Ag_2S/anti-Aβ/BSA (f), and ITO/SnO_2/SnS_2/Ag_2S/anti-Aβ/BSA/Aβ (g).

3.3. Optimization of experimental conditions

In order to obtain the best analytical performance for Aβ, the experimental conditions including the concentration of SnO_2, SnS_2, $AgNO_3$, the modification method of materials, the light intensity, the pH of PBS and the concentration of AA have been optimized (Dai et al., 2018; Wang et al., 2017d).

The effect of the SnO_2 concentration on the photocurrent responses was examined in the range from 1.0 to 3.5 mg mL^{-1}. As shown in Fig. 5A, it was found that the photocurrent value was maximum when the concentration was at 3.0 mg mL^{-1}. It is inferred that, at the appropriate concentration, the SnO_2 can accelerate the transmission of electrons and enlarge the contact surface of materials. However, when the concentration increased, the surface defect of materials hindered the transmission of electrons and the absorption of light, leading to the decrease of photocurrent signal. Actually, when the concentration was

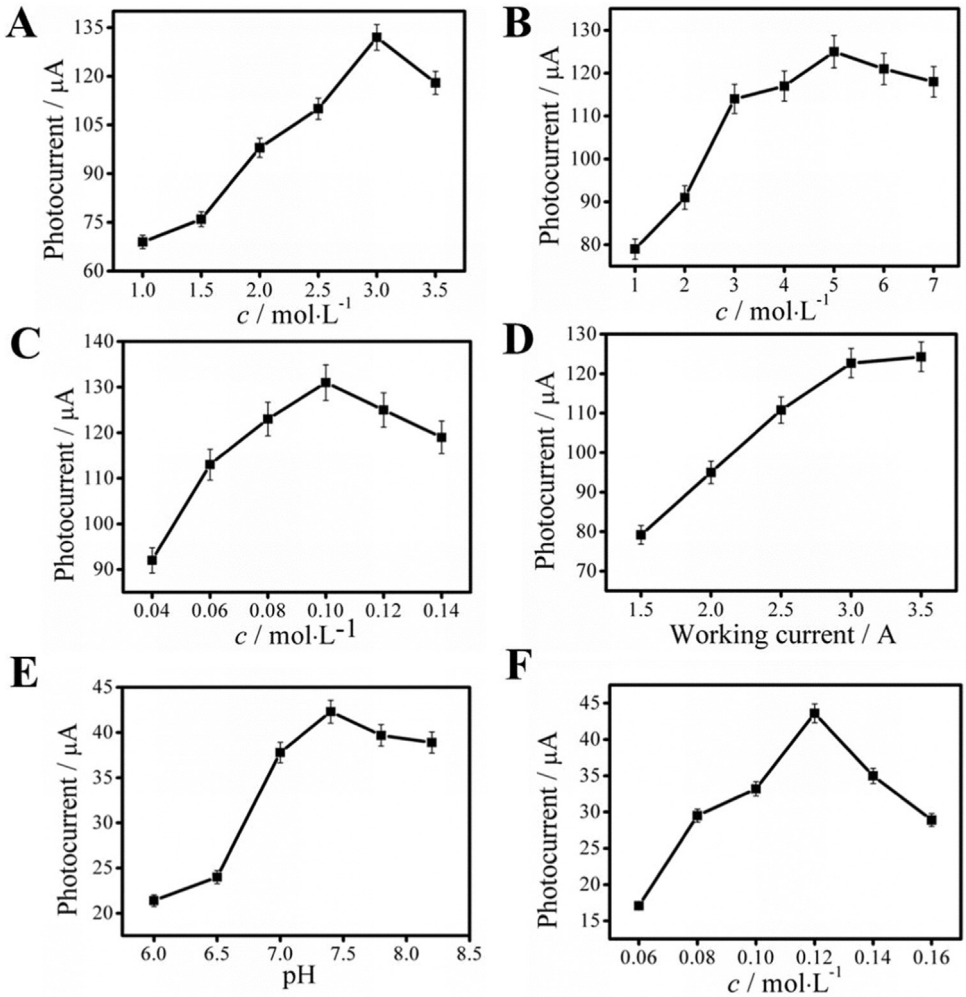

Fig. 5. Optimization of experimental conditions: (A) concentration of SnO_2; (B) concentration of SnO_2; (C) concentration of $AgNO_3$; (D) intensity of the light source; (E) pH on the photocurrent response of the immunosensor; (F) concentration of AA in the PBS buffer solution on the photocurrent response of the immunosensor. The applied potential was 0 V. Error bar = SD (n = 3).

too high, the resistance of the material was greater than the conductivity (Xing et al., 2018). Thus, the concentration of 3.0 mg mL^{-1} was chosen as the optimal concentration of SnO_2 in this study. Similarly, the experimental results showed that when the concentration of SnS_2 was 5.0 mg mL^{-1}, the current response reached the maximum (Fig. 5B).

In addition, to prepare ITO/SnO_2/SnS_2 electrode, the method of mixing SnO_2 and SnS_2 firstly was better than dropping layer by layer, leading to a higher photocurrent as shown in Fig. S3. This may be due to the fact that the ultrasound can make the mixing of materials more homogeneous, resulting in the tight combination of SnO_2 and SnS_2, further leading to changes of its physical performance. Therefore, the method of mixing SnO_2 and SnS_2 at the concentration ratio of 3:5 firstly by ultrasound was selected for the modification of the ITO electrode.

Ag_2S nanoparticles were in-situ growth on the surface of SnO_2/SnS_2 by reacting $AgNO_3$ and Na_2S solution in this experiment. Therefore, the concentration of $AgNO_3$ had an important influence on the photocurrent responses. Fig. 5C showed that the photocurrent responses increased as the concentration of $AgNO_3$ ranged from 0.02 to 0.10 mol L^{-1} and then slightly decreased, which was perhaps because that the amount of Ag_2S formed on the surface of SnO_2/SnS_2 reached saturation. More Ag_2S nanoparticles could hinder the electron transfer because of lower conductivity caused by thicker materials, and also lead to the high ratio of recombination of photo-generated e^-/h^+ because of the narrow band-gap of Ag_2S nanoparticles. Therefore, 0.10 mol L^{-1} of $AgNO_3$ was used in the subsequent experiment.

Meanwhile, light intensity also played an important role in the generation of photocurrent signal in PEC sensors. Hereinto, the full-wavelength LED lights acted as light sources, and the change in light intensity was achieved by changing the working current of the instrument. It can be observed from Fig. 5D that when the working current was 3.0 A, the photocurrent signal produced by the material was strong enough, and then reached a platform. Thus, the whole experiments in this study were carried out at the working current of 3.0 A.

The pH value of the buffer solution was also investigated. The overly acidic or alkaline detection surroundings might damage the activity of the immobilized protein. As shown in Fig. 5E, the photocurrent of the PEC immunosensor reached the maximum at pH 7.4, which was measured in PBS solutions with different pH ranging from 6.0 to 8.2. It could be explained that detection surroundings of pH 7.4 PBS solution were similar with the physiological environment and fit for the activity of the immobilized protein (Fan et al., 2018). Therefore, pH 7.4 was selected as the optimum value for PEC measurement.

Furthermore, AA was used as an electron donor to suppress the e^-/h^+ recombination, which had an important influence on the photocurrent response. As shown in Fig. 5F, the photocurrent responses increased firstly and then decreased with the increasing AA concentration from 0.06 to 0.16 mol L^{-1}. The decrease in photocurrent at higher AA concentration could be attributed to the quenched absorbance of the electrolyte solution, which thus decreased the light intensity and formation efficiency of excited electron-hole center (Kang et al., 2010). Therefore, 0.12 mol L^{-1} of AA in the PBS buffer solution (pH 7.4) was selected for Aβ analysis.

3.4. Analytical performance of the PEC immunosensor

Under the optimal conditions, the developed PEC immunosensor was applied to detect different concentrations of Aβ. As shown in time-based photocurrent curves (Fig. 6A), the photocurrent decreased with the increase of the concentration of Aβ. Fig. 6B showed the linear relationship related to the logarithmic values of Aβ concentration from 0.5 pg mL^{-1} to 100 ng mL^{-1} with low LOD of 0.17 pg mL^{-1} and LOQ of 0.56 pg mL^{-1} (calculation details see Supplementary material). The regression equation of the calibration curve was I = 42.3380–4.8324 lg c, with correlation coefficient of 0.9977, where I (μA) was the peak current of the immunosensor and c (ng mL^{-1}) was the concentration of Aβ. Compared with some other reported methods for the detection of Aβ (Table S1), the PEC immunosensor we fabricated can reach much wider linear range and lower LOD.

3.5. Stability, reproducibility and selectivity

The stability of the fabricated immunosensor was shown in Fig. 6C. The photocurrent response of the immunosensor was repeated 18 times on/off irradiation cycles for 400 s with incubated 10 ng mL^{-1} Aβ. There was no noticeable variation occurred, indicating that the PEC immunosensor possessed stable photocurrent response for Aβ detection. For the storage stability, the prepared immunosensor was stored in a refrigerator at 4 °C for 3 weeks. 94.8% of its initial photocurrent response was obtained for the detection of Aβ, showing the satisfactory storage stability of the prepared immunosensor.

To investigate the reproducibility of the PEC immunosensor, five ITO electrodes were assessed by the determination of 1 ng mL^{-1} Aβ under the same conditions. The relative standard deviation (RSD) of the measurements for the five electrodes was 1.8%, indicating that the proposed PEC immunosensor had quite good reproducibility.

To evaluate the selectivity of the fabricated PEC immunosensor, interfering substances of CEA, PSA, insulin and other subtype of Aβ like $Aβ_{1–40}$ and $Aβ_{1–28}$ were selected for the test. The solution of the target Aβ ($Aβ_{1–42}$, 1 ng mL^{-1}) containing interfering substances (100 ng mL^{-1}) were measured by the designed immunosensor and the results were shown in Fig. 6D. No distinct interferential photocurrent signal was observed when 100 ng mL^{-1} of CEA, PSA, insulin, $Aβ_{1–40}$ and $Aβ_{1–28}$ were incubated on the modified electrode respectively in the presence or absence of Aβ, which illustrated excellent selectivity and specificity of the PEC immunosensor for target Aβ.

3.6. Application of the immunosensor in human serum

To evaluate the practical applications of the prepared PEC immunosensor, the measurement of different concentrations of Aβ (0.10, 0.20, 0.50 ng mL^{-1}) in different human blood serum samples obtained from Hospital of University of Jinan were studied by standard addition methods. As shown in Table S2, the relative standard deviation (RSD) was in the range of 1.5–3.6%, and the recoveries of the samples were in the range of 97–104%. In order to further validate the applicability of the label-free PEC immunosensor in clinical practice, a comparative experiment with the commercialized available enzyme-linked immunosorbent assay (ELISA) method for the detection of Aβ in human serum sample was also conducted. These data revealed a good agreement between the two analytical methods, which indicated that the proposed PEC immunosensor has promising analytical application in blood sample detection.

4. Conclusion

In this study, a novel label-free PEC immunosensor based on SnO_2/SnS_2/Ag_2S nanocomposites was proposed for ultrasensitive detection of Aβ. As the matrix for the sensing electrode, SnO_2/SnS_2/Ag_2S nanocomposite could significantly enhance the photocurrent intensity due to its excellent properties of adequate absorption of light energy, ultrafast electron transfer, and effective inhibition of charge recombination. Thanks to the superior photoelectrochemical property of SnO_2/SnS_2/Ag_2S, the proposed immunosensor could realize the detection of Aβ with excellent sensitivity, selectivity, reproducibility and stability. A linear range of 0.5 pg mL^{-1} to 100 ng mL^{-1} was achieved with low LOD of 0.17 pg mL^{-1} and LOQ of 0.56 pg mL^{-1}, respectively. In addition, this proposed immunosensor was more convenient and economical for operation, which can constitute a novel approach to monitor biochemical effects of AD treatments and facilitate the clinical diagnosis since biomarker levels are significantly related with stage of AD. Furthermore, the proposed immunosensor may find promising

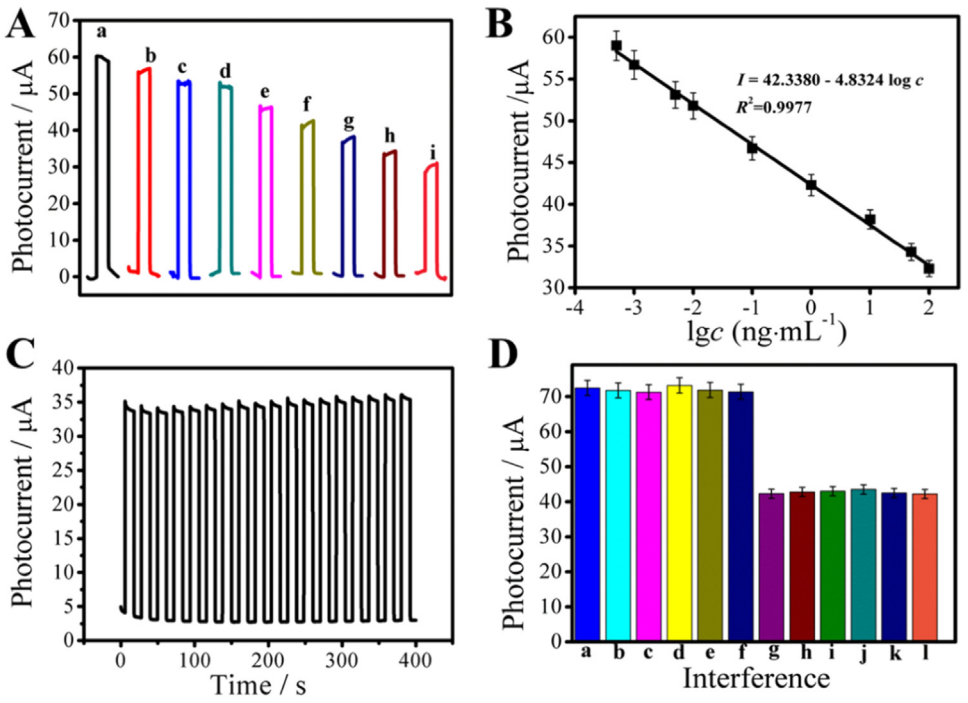

Fig. 6. (A) PEC responses of as-fabricated PEC immunosensor with different concentrations of Aβ: (a–i) 0.0005, 0.001, 0.005, 0.01, 0.1, 1, 10, 50, 100 ng mL^{-1}; (B) The logarithmic calibration curve of the PEC immunosensor for the detection of different concentrations of Aβ, Error bar = SD (n = 3); (C) Time-based photocurrent responses of the PEC immunosensor under several on/off irradiation cycles for 400 s, $c_{Aβ}$ = 1.0 ng mL^{-1}; (D) Selectivity of the PEC immunosensor for detecting Aβ: Blank (a), 100 ng mL^{-1} CEA (b), 100 ng mL^{-1} PSA (c), 100 ng mL^{-1} insulin (d), 100 ng mL^{-1} $Aβ_{1–40}$ (e), 100 ng mL^{-1} $Aβ_{1–28}$ (f), 1.0 ng mL^{-1} Aβ (g), 1.0 ng mL^{-1} Aβ + 100 ng mL^{-1} CEA (h), 1.0 ng mL^{-1} Aβ + 100 ng mL^{-1} PSA (i), 1.0 ng mL^{-1} Aβ + 100 ng mL^{-1} insulin (j), 1.0 ng mL^{-1} Aβ + 100 ng mL^{-1} $Aβ_{1–40}$ (k), 1.0 ng mL^{-1} Aβ + 100 ng mL^{-1} $Aβ_{1–28}$ (l). The applied potential was 0 V. Error bar = SD (n = 3).

applications in the detection of other disease-related biomarkers, environmental pollutants and other biomolecules. Whereas only single component could be analyzed by the proposed immunosensor, the detection of multiple components by designing new strategy and constructing novel platform will be conducted in future work.

Acknowledgements

This study was supported by the National Natural Science Foundation of China (Nos. 21575050, 21777056), National Key Scientific Instrument and Equipment Development Project of China (No.21627809), and Qin Wei thanks the Special Foundation for Taishan Scholar Professorship of Shandong Province (No. ts20130937) and UJN.

Appendix A. Supporting information

Supplementary data associated with this article can be found in the online version at doi:10.1016/j.bios.2018.08.026.

References

Banerjee, S., Mohapatra, S.K., Das, P.P., Misra, M., 2008. Chem. Mater. 20 (21), 6784–6791.
Cao, T., Li, Y., Wang, C., Shao, C., Liu, Y., 2011. Langmuir 27, 2946–2952.
Carneiro, P., Loureiro, J., Delerue-Matos, C., Morais, S., Pereira, Md.C., 2017. Sens. Actuators B-Chem. 239, 157–165.
Cummings, J.L., 2004. New Engl. J. Med. 351 (1), 56–67.
Dai, X., Deng, W., You, C., Shen, Z., Xiong, X., Sun, X., 2018. Anal. Methods 10 (15), 1680–1684.
Elangovan, E., Ramamurthi, K., 2003. J. Optoelectron. Adv. Mater. 5 (1), 45–54.
Fan, D., Bao, C., Khan, M.S., Wang, C., Zhang, Y., Liu, Q., Zhang, X., Wei, Q., 2018. Biosens. Bioelectron. 106, 14–20.
Fan, D., Wu, D., Cui, J., Chen, Y., Ma, H., Liu, Y., Wei, Q., Du, B., 2015. Biosens. Bioelectron. 74, 843–848.
Han, Q., Wang, R., Xing, B., Zhang, T., Khan, M.S., Wu, D., Wei, Q., 2018. Biosens. Bioelectron. 99, 493–499.
Hu, T., Zheng, Y.-N., Li, M.-J., Liang, W.-B., Chai, Y.-Q., Yuan, R., 2018. Anal. Chem. 90 (10), 6096–6101.
Huang, H., Ju, X., Li, H., Qu, B., Wang, T., 2018. J. Alloy. Compd. 744, 375–380.
Jiang, M.-H., Lu, P., Lei, Y.-M., Chai, Y.-Q., Yuan, R., Zhuo, Y., 2018. Electrochim. Acta 271, 464–471.
Kang, Q., Yang, L., Chen, Y., Luo, S., Wen, L., Cai, Q., Yao, S., 2010. Anal. Chem. 82, 9749–9754.
Li, F., Chen, L., Knowles, G.P., Macfarlane, D.R., Zhang, J., 2017. Angew. Chem. Int. Ed. 56 (2), 505–509.
Liang, Y., Tsubota, T., Mooij, L.P.A., Krol, R. vd, 2011. J. Phys. Chem. C 115 (35), 17594–17598.
Liu, X., Pan, L., Lv, T., Zhu, G., Lu, T., Sun, Z., Sun, C., 2011. RSC Adv. 1 (7), 1245–1249.
Liu, Z., Ji, G., Guan, D., Wang, B., Wu, X., 2015. J. Colloid Interfaces Sci. 457, 1–8.
Lv, S., Zhang, K., Zeng, Y., Tang, D., 2018. Anal. Chem. 90 (11), 7086–7093.
Ma, C., Liu, F., Yang, H., Ge, S., Yu, J., Yan, M., Song, X., 2014. Sens. Actuators B-Chem. 195, 423–430.
Park, S., Park, J., Selvaraj, R., Kim, Y., 2015. J. Ind. Eng. Chem. 31, 269–275.
Qiu, Z., Shu, J., Tang, D., 2018. Anal. Chem. 90 (1), 1021–1028.
Reiman, E.M., 2016. Nature 537 (7618), 36–37.
Selkoe, D.J., Hardy, J., 2016. EMBO Mol. Med. 8, 595–608.
Shi, L., Lin, H., 2011. Langmuir 27 (7), 3977–3981.
Thapa, A., Jett, S.D., Chi, E.Y., 2016. ACS Chem. Neurosci. 7, 56–68.
Wang, H., Peng, L., Chai, Y., Yuan, R., 2017a. Anal. Chem. 89 (20), 11076–11082.
Wang, Q., Kou, X., Liu, C., Zhao, L., Lin, T., Liu, F., Yang, X., Lin, J., Lu, G., 2018a. J. Colloid Interfaces Sci. 513, 760–766.
Wang, R., Ma, H., Zhang, Y., Wang, Q., Yang, Z., Du, B., Wu, D., Wei, Q., 2017b. Biosens. Bioelectron. 96, 345–350.
Wang, S., Huang, J., Zhao, Y., Wang, S., Wu, S., Zhang, S., Huang, W., 2006. Mater. Lett. 60, 1706–1709.
Wang, X., Xu, R., Sun, X., Wang, Y., Ren, X., Du, B., Wu, D., Wei, Q., 2017c. Biosens. Bioelectron. 96, 239–245.
Wang, Y., Zhao, G., Li, X., Liu, L., Cao, W., Wei, Q., 2018b. Biosens. Bioelectron. 101, 290–296.
Wang, Z., Xie, F., Liu, Z., Du, G., Asiri, A.M., Sun, X., 2017d. Chem. -Eur. J. 23, 16179–16183.
Xie, F., Liu, T., Xie, L., Sun, X., Luo, Y., 2018. Sens. Actuators B-Chem. 255, 2794–2799.
Xie, Q., Zhou, H., Lv, Z., Liu, H., Guo, H., 2017. J. Mater. Chem. A 5, 6299–6309.
Xing, B., Zhu, W., Zheng, X., Zhu, Y., Wei, Q., Wu, D., 2018. Sens. Actuators B-Chem. 265, 403–411.
Xiong, X., You, C., Cao, X., Pang, L., Kong, R., Sun, X., 2017. Electrochim. Acta 253, 517–521.
Yan, S., Liang, X., Song, H., Ma, S., Lu, Y., 2018. Ceram. Int. 44, 358–363.
Yang, W., Zhang, L., Hu, Y., Zhong, Y., Wu, H.B., Lou, X.W., 2012. Angew. Chem. Int. Ed. 51 (46), 11501–11504.
Yao, L., Zhang, Y., Li, J., Chen, Y., 2014. Sep. Purif. Technol. 122, 1–5.
Yin, M., Yao, Y., Fan, H., Liu, S., 2018. J. Alloy. Compd. 756, 322–331.
Yun, G., Balamurugan, M., Kim, H.S., Ahn, K.S., Kang, S.H., 2016. J. Phys. Chem. C 120 (11), 5906–5915.
Zhang, G., Chen, D., Li, N., Xu, Q., Li, H., He, J., Lu, J., 2018. J. Colloid Interfaces Sci. 514, 306–315.
Zhang, J., Zhu, H., Zheng, S., Pan, F., Wang, T., 2009. ACS Appl. Mater. Interfaces 1 (10), 2111–2114.
Zhang, Y., Du, Z., Li, K., Zhang, M., Dionysiou, D.D., 2011. ACS Appl. Mater. Interfaces 3 (5), 1528–1537.
Zhao, W.-W., Ma, Z.-Y., Yan, D.-Y., Xu, J.-J., Chen, H.-Y., 2012. Anal. Chem. 84 (24), 10518–10521.
Zhou, W., Liu, H., Wang, J., Liu, D., Du, G., Cui, J., 2010. ACS Appl. Mater. Interfaces 2 (8), 2385–2392.
Zhou, X., Zhou, T., Hu, J., Li, J., 2012. CrystEngComm 14 (17), 5627–5633.